The FEBS Journal

FEBS PRESS science publishing by scientists

Biophysical investigation of the molecular interaction between minichromosome maintenance protein 6 and Bloom syndrome helicase

Min June Yang, Haeun Lee, Donguk Kang and Chin-Ju Park

Department of Chemistry, Gwangju Institute of Science and Technology, Gwangju, Korea

Keywords
Bloom syndrome protein; intrinsically disordered region; MCM6 WHD; NMR; protein–protein interaction

Correspondence
C.-J. Park, Department of Chemistry, Gwangju Institute of Science and Technology, Gwangju 61005, Korea
Tel: +82 62 715 3630
E-mail: cjpark@gist.ac.kr

Min June Yang and Haeun Lee contributed equally to this article.

(Received 2 October 2024, revised 14 January 2025, accepted 17 February 2025)

doi:10.1111/febs.70047

The minichromosome maintenance protein (MCM) complex and Bloom syndrome helicase (BLM) are crucial components in DNA replication and cell division. MCM, a hexameric helicase that unwinds double-stranded DNA, serves as an important diagnostic and prognostic biomarker for cancer cells and a target for anticancer drug development. BLM, associated with G-quadruplex structures, is another key helicase in maintaining genomic stability. In this study, we investigate the interaction between MCM6 and BLM at the atomic level, as their expression levels are highly correlated in various cancer types, with elevated levels indicating poor prognosis. To elucidate the molecular basis of MCM6/BLM interaction, we employed fluorescence polarization anisotropy analysis, NMR chemical shifts perturbation analysis (CSP), and paramagnetic relaxation enhancement (PRE) experiments. MCM6 binding domain (MBD) C and D exhibit similar binding affinities to MCM6 winged-helix domain (WHD). However, significant CSPs with MBD-D and PRE experiments suggested that MBD-D is closer to MCM6 WHD than MBD-C. Despite both proteins containing numerous negatively charged residues, hydrophobic interactions govern the association between MCM6 WHD and BLM MBD-D. This biophysical characterization of the MCM6/BLM interaction provides new insights into their functional relationship and challenges existing models. Our findings reveal that MCM6 binds BLM at a different site than its other known partner chromatin licensing and DNA replication factor. Understanding these protein–protein interactions at the molecular level may contribute to the development of novel anticancer therapies targeting the MCM6/BLM interaction.

Introduction

Gene instability, a potential precursor to cancer development, primarily stems from errors in the DNA repair processes [1–3]. Among various DNA repair mechanisms, homologous recombination (HR) [4] involves the formation of Holliday junctions [5], which are key structural intermediates that help prevent gene

Abbreviations
a.a., amino acids; BLM, Bloom syndrome helicase; Cdt1, chromatin licensing and DNA replication factor; CSP, chemical shift perturbation; DMSO, dimethyl sulfoxide; EDTA, ethylenediaminetetraacetic acid; FITC, fluorescein isothiocyanate; FPA, fluorescence polarization anisotropy; GTEx, Genotype-Tissue Expression database; HR, homologous recombination; HRDC, helicase core and an RNase D C-terminal domain; HSQC, heteronuclear single quantum coherence; IC_{50}, half maximal inhibitory concentration; K_d, dissociation constant; MBD, MCM6 binding domain; MCM, minichromosome maintenance protein; MTSL, (1-oxyl-2,2,5,5-tetramethyl-3-pyrroline-3-methyl) methanesulfonate; NMR, nuclear magnetic resonance; PRE, paramagnetic relaxation enhancement; PTM, post-translational modification; *R*, Pearson's rho correlation; RQC, RecQ C-terminal domain; WHD, winged-helix domain.

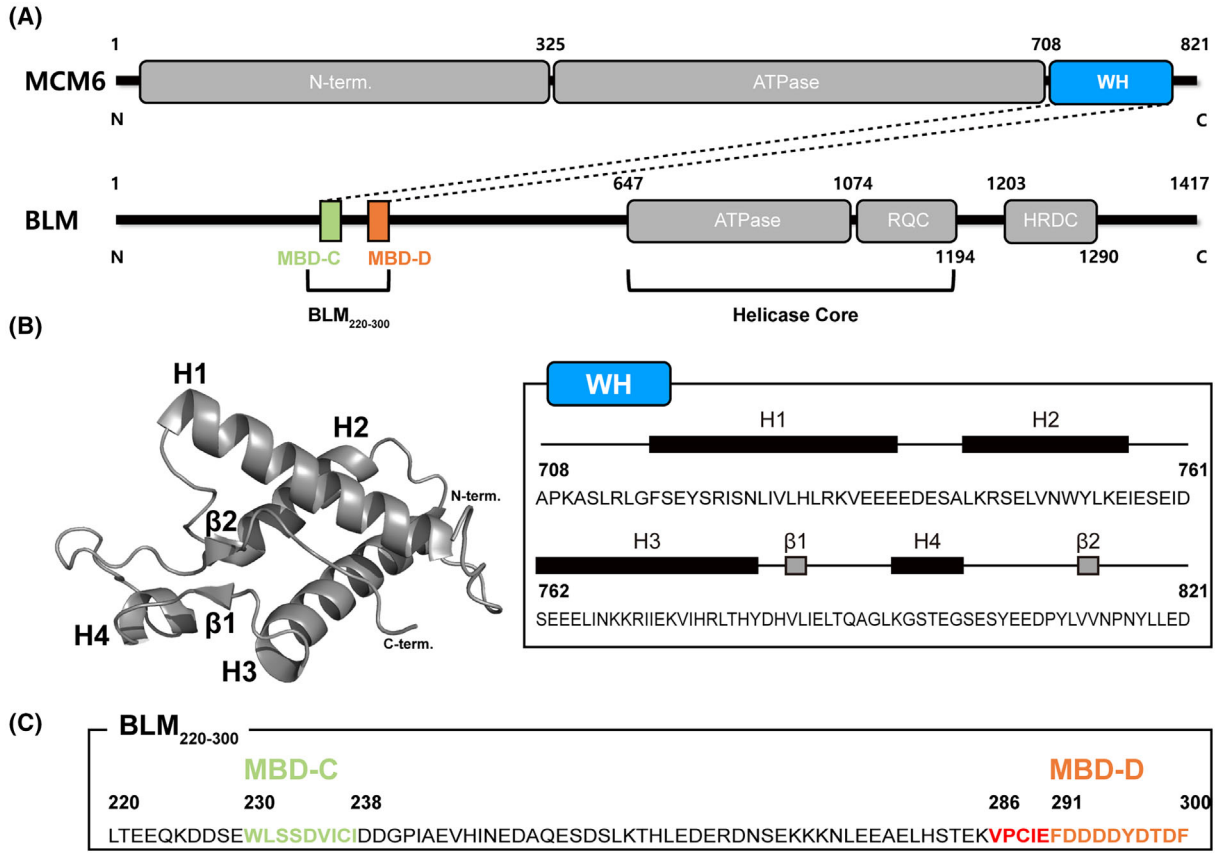

Fig. 1. Domain architecture and structural representation of MCM6 and BLM. (A) Domain structure of human MCM6 and BLM. Winged-helix (WH), MCM6 binding domain (MBD) C, and D, known to be involved in the interaction, are marked in blue, green, and orange, respectively. (B) NMR solution structure of MCM6 winged-helix domain (WHD) (PDB ID: 2KLQ [38]), with corresponding sequences and secondary structure elements. The structure was visualized using PYMOL [75]. (C) Sequence of $BLM_{220–300}$. WHD binding BLM peptides (BLM MBD-C; 230–238, BLM MBD-D; 291–300, and $BLM_{286–300}$; 286–300) examined in this study are shown, with their positions in the sequence indicated in green, orange, and red, respectively.

instability. Defects in DNA repair mechanisms, such as HR, have been related to various types of cancer, including breast and ovarian cancer. Mutations in the BRCA1 and BRCA2 genes impair the ability of cells to repair DNA double-strand breaks via HR, leading to the accumulation of genetic errors and the potential for malignant transformation [6,7]. As DNA is prone to both extrinsic and intrinsic damage, repair systems are indispensable for maintaining genomic integrity [1,8].

Minichromosome maintenance proteins (MCM) play essential roles in DNA repair, replication, and stability. MCM is crucial for the repair mechanism through the formation of HR response to DNA double-stranded breaks [9]. The MCM complex functions as a helicase that unwinds double-stranded DNA to single-stranded DNA in the nucleus and consists of six subunits [10–13]. Mutations in MCM proteins can lead to replication stress and genome instability, hallmarks of cancer [14,15]. Copy number variations and deletions of MCMs have been observed in various cancer cells, significantly accelerating cancer progression [16,17].

Results from The Cancer Genome Atlas and Gene Expression Omnibus analyses have shown exceptional expression levels of MCM6, one of the proteins constituting the MCM2-7 complex, in breast cancer [18–20], gastric cancer [21,22], renal cell carcinoma [23–25], hepatocellular carcinoma [26–29], and nonsmall cell lung carcinoma [30–32]. Several drugs targeting MCM subunits are currently in development [15,33]. Notably, high expression of MCM6 has been associated with lower survival rates and higher histological grades in nonsmall lung cancer and breast cancer [32,34].

MCM6 consists of three domains: the N-terminal domain (1–325 amino acids; a.a.), ATPase domain (326–707 a.a.), and winged-helix domain (WHD; 708–821 a.a.) (Fig. 1A). Among these, the WHD is

known to be involved in regulating helicase activity, facilitating the formation of the MCM complex, or regulating MCM complex activity through protein–protein interaction [35,36]. In particular, the MCM6 WHD plays a role in attaching the MCM complex to DNA replication origins through interaction with chromatin licensing and DNA replication factor (Cdt1) [37]. The WHD is structurally composed of four α-helices, two β-strands, and two loops, and it was figured out by NMR solution structure (PDB ID: 2KLQ [38], Fig. 1B).

Similarly, Bloom syndrome helicase (BLM) is involved in DNA repair, replication, and recombination. BLM is one of the five RecQ DNA helicase families in humans, which encodes a 3′ to 5′ DNA helicase [39]. Bloom syndrome, an autosomal recessive genetic disease, is caused by a defect in the BLM gene, which plays a crucial role in DNA replication and repair [40,41]. BLM facilitates HR in response to DNA double-stranded breaks [1,4,42] and is essential for the DNA replication mechanism [43–46]. BLM consists of two main domains: a disordered N-terminal tail (1–647 a.a.) and a C-terminal helicase domain (648–1417 a.a.) [5]. The C terminus of BLM is composed of a helicase core and an RNase D C-terminal domain (HRDC; 1208–1290 a.a.) [47], with the helicase core containing an ATPase [48,49] (Fig. 1A).

In addition to its role in HR, BLM functions as a G-quadruplex helicase. G-quadruplexes are highly stable secondary structures formed in G-rich regions of DNA [50]. BLM resolves these structures to prevent stalling of the replication fork and facilitate the smooth progression of DNA replication. The ability of BLM to unwind G-quadruplexes is critical for maintaining genome stability and preventing replication stress [51]. Overexpression of BLM has been observed in breast [52], prostate [52,53], colorectal [52,54], and lung [52] cancers.

The MCM6/BLM interaction is known to be a key interaction in the DNA repair process. The BLM helicase can be confirmed based on the highest expression level of BLM during the S phase [55,56]. In the case of DNA damage in the S and G1 phases, MCM6 binds to BLM at specific positions [55,57]. Physical interaction between MCM6 and BLM is required to maintain optimal G-quadruplex unwinding speed after DNA damage [56]. The activity of BLM helicase can increase the replication rate of normal cells [5,39]. Therefore, the MCM6/BLM interaction is important for replication stress response and replication repair caused by DNA double-strand breaks [3,47,58]. It also functions as a negative regulator of DNA replication rate [56].

The previous study investigated the binding site of BLM to MCM6 using truncated mutants of MCM6 and BLM. Three parts of BLM are known to be important for MCM6 binding, which comprise the MCM6 binding domain (MBD). $BLM_{83–90}$ (MBD-N) is known to interact with the N terminus of MCM6 in the G1 phase, while $BLM_{230–238}$ (MBD-C) and $BLM_{291–300}$ (MBD-D) interact with the MCM6 WHD in S phase [56]. The $BLM_{220–300}$ region has no secondary structure [59] and is a construct containing MBD-C and D (Fig. 1C). The intricate interplay between the MCM6 WHD and each MBD of BLM is indispensable for maintaining optimal DNA replication rates during repair processes. However, the precise binding sites within the MCM6 WHD have not been fully characterized.

Given that previous studies have established that both MCM6 and BLM are related to cancer, we investigated the correlation between the expression level of these two proteins through cohort analysis. Our results revealed that the expression levels of MCM6 and BLM are highly correlated in cancer cells, and cancer patients with high expression of both proteins have a poor prognosis. To address the gap in understanding the precise binding sites, we conducted an investigation utilizing NMR and fluorescence polarization anisotropy (FPA) assays. We successfully validated the binding site between MCM6 WHD and BLM MBD-D. MCM6 WHD, $BLM_{220–300}$, $BLM_{286–300}$, MBD-C, and D were used in the experiment (Fig. 1). This study provides crucial insights into the structural understanding of their intermolecular interaction, elucidating the molecular mechanisms underlying DNA repair processes and potentially offering new avenues for cancer research.

Results

MCM6 and BLM are highly correlated, and their high expressions are associated with poor prognoses in cancer

To investigate the correlation between MCM6 and BLM expression levels in cancer cells, we performed the UCSC XENA [60] analysis for MCM6 and BLM. Figure 2A,B illustrate that the expression levels of MCM6 and BLM were generally higher in the Pan-cancer database compared to the Genotype-Tissue Expression database (GTEx). Correlation between protein expression levels can provide valuable insight into the mechanisms underlying cancer development, progression, and treatment response. Understanding these correlations may help identify potential biomarkers for

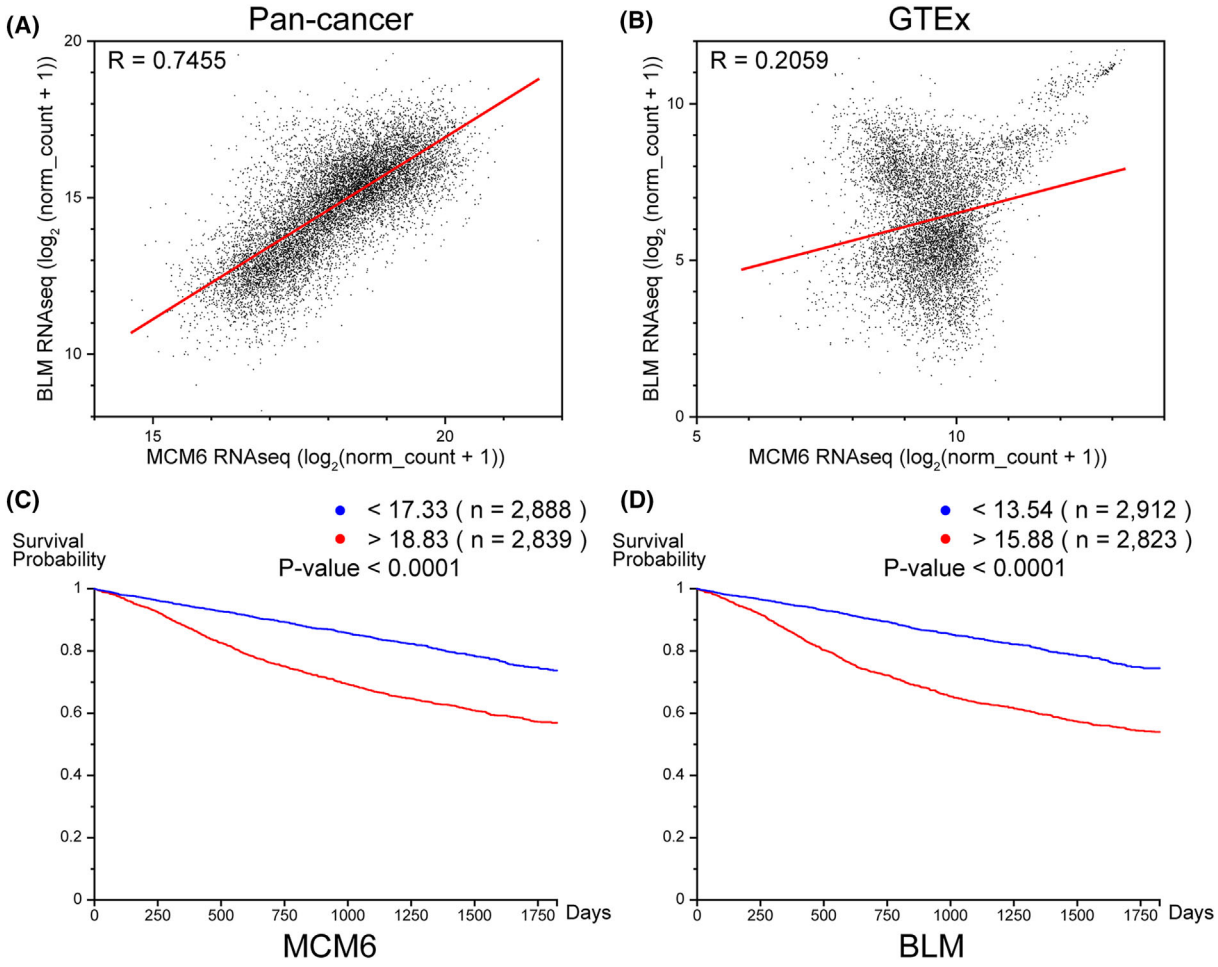

Fig. 2. Correlation between MCM6 and BLM expression in cancer and normal tissues. (A) Correlation of MCM6 and BLM expression in the Pan-cancer database ($n = 11\,768$). (B) Correlation of MCM6 and BLM expression in the Genotype-Tissue Expression database (GTEx, $n = 7819$). Linear regression and Pearson's rho (R) are indicated on each graph. Kaplan–Meier survival curves comparing patients with high (red) and low (blue) expression of (C) MCM6 or (D) BLM in the Pan-cancer database. These were plotted from the UCSC XENA.

cancer prognosis and therapeutic targets [61,62]. Pearson's rho correlation (R) was low at 0.2059 in GTEx but high at 0.7455 in Pan-cancer. The expression levels of MCM6 and BLM were correlated in cancer cells but not in normal cells, implying that the MCM6/BLM interaction is important for cancer cells.

Further, Kaplan–Meier estimator analysis was performed to assess the effect of the two proteins on cancer patients. Fig. 2C,D show the survival rate of cancer patients based on their MCM6 and BLM expression levels. Patients with high expression of both proteins had a poorer prognosis, with 5-year survival probabilities of 0.57 and 0.54, respectively. In contrast, patients with low expression levels of MCM6 and BLM had higher survival probabilities of 0.74 for both proteins.

In conclusion, our results indicate that MCM6 and BLM are significantly upregulated in cancer cells and are strongly correlated. When we examined the results by cancer type as well as Pan-cancer, we found that the expression levels of MCM6 and BLM were correlated in adrenocortical carcinoma (ACC), kidney renal clear cell carcinoma (KIRC), kidney renal papillary cell carcinoma (KIRP), mesothelioma (MESO), and lower grade glioma (LGG) and that they also had poor prognosis (Fig. S1). Additional studies are needed to elucidate the correlation between MCM6 and BLM across various cancer types. Elevated expression levels of these proteins are associated with poorer patient outcomes, suggesting their potential role as biomarkers for cancer prognosis and as targets for therapeutic intervention.

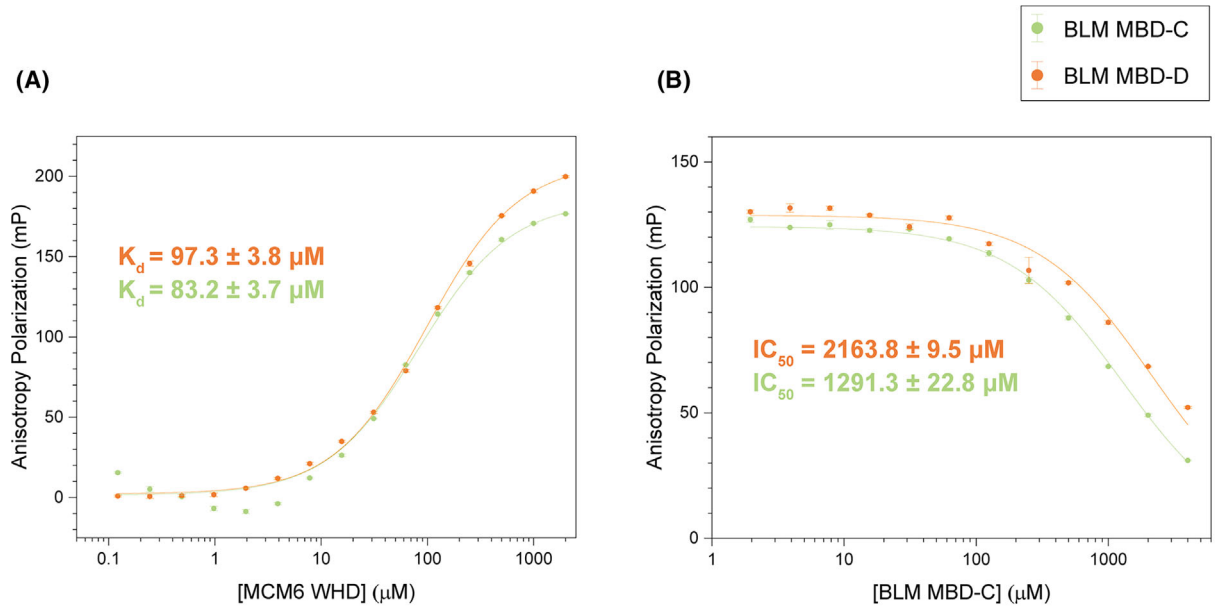

Fig. 3. Fluorescence polarization anisotropy (FPA) of MCM6 WHD binding to BLM peptides. (A) FPA of FITC-labeled BLM MCM6 binding domain (MBD) C and D titrated with MCM6 WHD. (B) Competitive FPA of FITC-labeled BLM MBD-C and D peptides in the presence of 200 μM MCM6 WHD, titrated by the MBD-C peptide. The K_d and IC_{50} values for each peptide are indicated in the graph. All measurements were performed in triplicate ($n = 3$), and error bars represent the standard deviation of the replicated results.

MBD-C and D show similar binding affinities but displace differently to MCM-6 WHD

Given the high correlation between MCM6 and BLM expression levels in cancer cells, we hypothesized that the molecular interaction between MCM6/BLM interaction is crucial for understanding cancer development. A previous study identified two regions of BLM (MBD-C and D) as binding sites for MCM6 WHD [56]. We conducted FPA experiments to measure the binding affinities of these two regions to the WHD. The MCM6 WHD C721S mutant, which has a similar structure and properties to the wild-type of MCM6 WHD [37,38], was used in our experiments and will be referred to as MCM6 WHD hereafter. MCM6 WHD was titrated to fluorescein isothiocyanate (FITC) labeled-MBD-C or D peptides to determine binding affinity.

Figure 3A shows the results of FPA assays of the FITC-labeled BLM MBD-C and D peptides with MCM6 WHD. Through curve fitting, the dissociation constant (K_d) of the MCM6 WHD-BLM MBD-C complex was determined to be 83.2 ± 3.7 μM, while the K_d of the MCM6 WHD-BLM MBD-D complex was determined to be 97.3 ± 3.8 μM. We performed a competitive FPA assay to compare MBD-C and D binding preferences for MCM6 WHD in the presence of both peptides. The results indicate that MBD-C competes 1.7 times more effectively with itself than with MBD-D, suggesting that MBD-D is less susceptible to displacement by MBD-C (Fig. 3B). At 4 mM MBD-C, the FITC-BLM-MBD-C complex retained approximately 40% of the initial binding, while FITC-BLM-MBD-D retained around 53%.

Previous studies have shown that MCM6 and BLM do not interact in immunoprecipitation experiments when either MBD-C or D regions are deleted [56]. Notably, mutating both regions weakened the interaction between MCM6 and BLM, but mutating MBD-C during cell division had a more significant impact than mutating MBD-D [56]. Our FPA results demonstrated that the two MBD regions (C and D) bind to MCM6 WHD with similar affinities. Since our experiment focused on the WHD of MCM6 and the MBD-C and D regions of BLM, our findings may differ from those of the previous study [56], which investigated the interactions of the full-length proteins and the effects of alanine mutations in different MBD regions. This suggests that *in vitro* interactions observed at the domain-level may not fully capture the complexity of full-length protein interactions during cell division. This suggests that factors other than the direct interaction of the two proteins may influence their behavior during cell division.

Helix 1 and C terminus of WHD are important for MBD-D binding

To investigate the structural aspects of MCM6 WHD binding with MBD-C and D, we performed NMR heteronuclear single quantum coherence (HSQC) titration experiments. The experiment was conducted using the existing assignment of MCM6 WHD reported in a previous study (BMRB: 16396 [38]). Despite the moderate binding affinity observed in FPA experiments ($K_d = 83.2 \pm 3.7\,\mu M$), no significant chemical shift changes were observed during the titration of MCM6 WHD with BLM MBD-C (Fig. S2). This unexpected result is likely due to the low solubility of MBD-C under NMR experimental conditions.

In contrast to MBD-C, significant CSPs were observed in the HSQC experiments with MBD-D. Figure 4A shows the average backbone NH chemical shift perturbation (CSP) values ($\Delta\delta_{avg}$) of ^{15}N labeled MCM6 WHD during binding to BLM MBD-D. CSP values exceeding two standard deviations above the mean $\Delta\delta_{avg}$ were observed in residues within helix 1 and the C terminus of MCM6 WHD (Fig. 4B). The most perturbed peaks, L715, V734, L785, L787, I788, E807, and N814, are shown in Fig. S3. The titration experiment revealed that the interaction between MCM6 WHD and BLM MBD-D occurs at a fast exchange rate on the NMR timescale. Furthermore, the results indicate that hydrophobic residues are primarily involved in the interaction between MCM6 WHD and BLM MBD-D. This suggests that although most of the MBD-D sequence is negatively charged (isoelectric point (pI): 3.17), conserved aromatic residues ($F_{291}Y_{296}F_{300}$) could play a crucial role in the interaction with MCM6.

PRE analysis reveals MBD-D is closer to MCM6 WHD than MBD-C

Since we could not observe CSPs for MBD-C due to its low solubility, we took an alternative approach using paramagnetic relaxation (PRE) enhancements. To determine which region is closer to MCM6 WHD, we prepared the $BLM_{220–300}$ construct containing both BLM MBD-C and D. Since two cysteine residues were present in $BLM_{220–300}$, we prepared $BLM_{220–300}$ C237S and $BLM_{220–300}$ C288S for (1-oxyl-2,2,5,5-tetramethyl-3-pyrroline-3-methyl) methanesulfonate (MTSL) labeling at only one cysteine residue. C237 is included in the MBD-C region (230–238), and C288 is anterior to the MBD-D (291–300) region (Fig. 5A,B).

Paramagnetic labeling with MTSL at C288, anterior to the MBD-D region, resulted in a significant decrease in intensity for residues L714, G716, S721, S724, and V728 from helix 1 of MCM6 WHD (Fig. 5A). This is consistent with our CSP analysis results. However, no significant decrease in intensity was observed when MTSL was labeled at C237 located in the MBD-C region (Fig. 5B). These findings suggest that the MBD-D region is close to helix 1 of the MCM6 WHD, while the MBD-C region is not in close proximity. In a situation where both MBD-C and D are present, MBD-D appears to be preferred for binding to the WHD. No significant PRE reduction effect was observed in the WHD C terminus, where the chemical shift changes were observed in HSQC

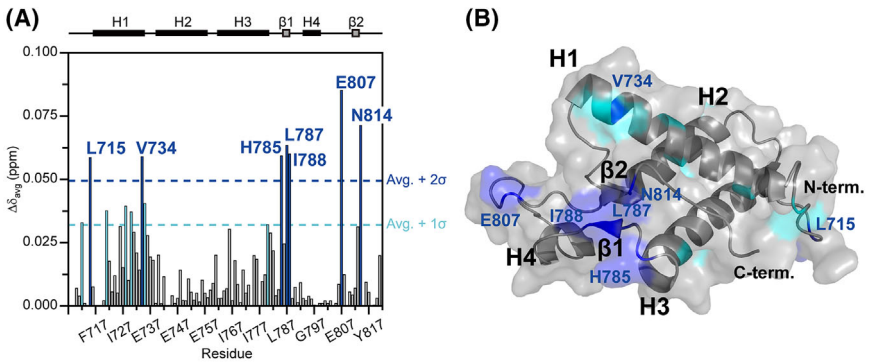

Fig. 4. NMR Chemical shift perturbation (CSP) analysis of MCM6 winged-helix domain (WHD) binding to BLM MBD-D. (A) Average chemical shift changes of MCM6 WHD upon BLM MCM6 binding domain D peptide binding. Residues with $\Delta\delta_{avg}$ exceeding one standard deviation (cyan bar) and two standard deviations (blue bar) are highlighted. Secondary structure elements are shown at the top of the graph. NMR titration was performed once ($n = 1$) due to sample limitations. Average (Avg.) and standard deviations (σ) were calculated from the CSPs of all assigned residues. (B) NMR solution structure of WHD (PDB ID: 2KLQ [38]) is color-coded based on CSP data. The structure was visualized using PYMOL [75].

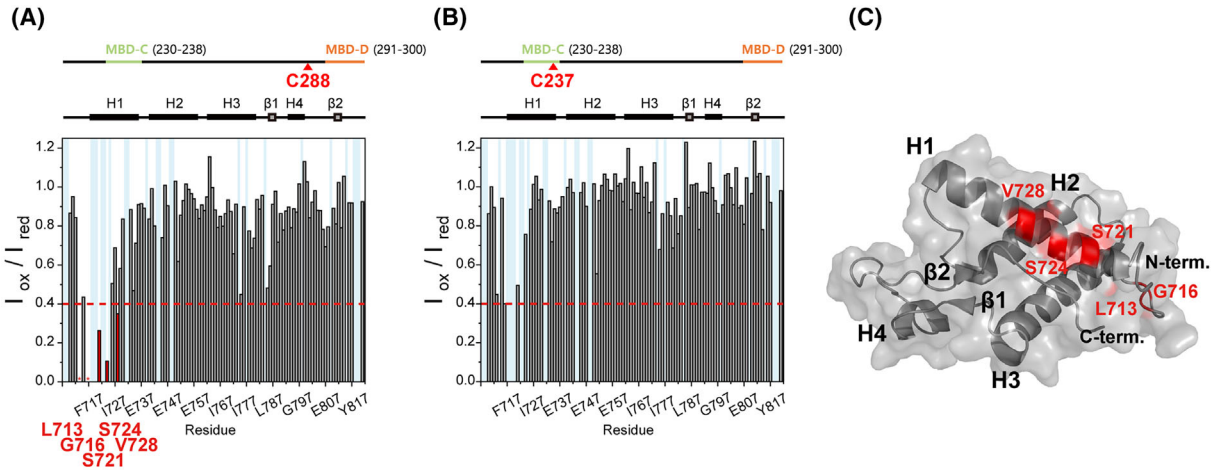

Fig. 5. Paramagnetic relaxation enhancement (PRE) analysis of MCM6 winged-helix domain (WHD) interaction with $BLM_{220–300}$. PRE experiment results of ^{15}N labeled MCM6 WHD with paramagnetically labeled $BLM_{220–300}$ on (A) C288 and (B) C237. Residues with a PRE ratio (I_{ox}/I_{red}) less than 0.4 are indicated in red, and disappeared peaks are marked with a red asterisk. Secondary structure elements are shown at the top of the graph. Light blue bars indicate unassigned residues. (C) NMR solution structure of WHD (PDB ID: 2KLQ [38]) is color-coded based on PRE data. The structure was visualized using PYMOL [75]. PRE experiment was performed once ($n = 1$) due to sample limitations.

titration. This is likely due to the distance being greater than the effective range for PRE (25–35 Å) [63] between C288 and the WHD C terminus, or because the chemical shift changes observed in HSQC titration had a more significant effect on the unstructured C terminus.

The PRE results mapped onto the existing NMR solution structure of MCM6 WHD (PDB ID: 2KLQ [38]) are shown in Fig. 5C. It can be seen that helix 1 is primarily involved in binding to BLM MBD-D. MBD-D appears to occupy a different binding site from Cdt1, previously known to bind to MCM6 (Fig. S4A,B) [38]. Because Cdt1 has a high positive charge (pI: 10.27), it is known to interact electrostatically with MCM6 WHD (pI: 4.62), which has an overall negative charge (Fig. S4C). On the other hand, BLM MBD-D (pI: 3.17), which has many acidic residues, is predicted to maintain binding through interactions between hydrophobic residues despite having similar charge to MCM6 WHD. The regions important for MBD-D binding generally have hydrophobic surfaces (Fig. S4D).

Nonconserved region of BLM plays an important role in MCM6 WHD binding

Our results from multiple biophysical approaches consistently demonstrated the importance of MBD-D interaction with WHD. While FPA experiments showed similar binding affinities for both MBD-C and D, PRE analyses revealed that MBD-D is positioned close to helix 1 of MCM6 WHD. However, the potential involvement of nonconserved BLM regions other than MBD-C and D in the interaction had not been previously studied. To investigate the role of the nonconserved region, we performed CSP analysis by titrating unlabeled MCM6 WHD on ^{15}N labeled $BLM_{220–300}$.

We previously reported the backbone atom chemical shift assignments of the $BLM_{220–300}$ (BMRB: 52084 [59]), and the experiment was conducted using these existing assignments. The $\Delta\delta_{avg}$ values of ^{15}N labeled $BLM_{220–300}$ during binding to MCM6 WHD are shown in Fig. 6. With increasing molar ratios of MCM6 WHD, ^{1}H-^{15}N cross peaks of V286, C288, I289, E290, and F291 are shown in Fig. S5. We observed that the interaction occurs at a fast exchange rate on the NMR timescale, similar to our observations in Fig. S3.

Following the experiment, we observed CSP values exceeding two standard deviations from the mean $\Delta\delta_{avg}$ value in the C terminus corresponding to the MBD-D region. The average $\Delta\delta_{avg}$ value of the MBD-D region was 0.025 ppm, which was twice as high as the overall average value of 0.012 ppm. This is consistent with the results of our previous experiments. However, we found that the $\Delta\delta_{avg}$ values in the $BLM_{286–290}$ region ($_{286}$VPCIE$_{290}$) located immediately upstream of MBD-D were even larger (0.053 ppm). This suggests that the nonconserved $BLM_{286–290}$ region

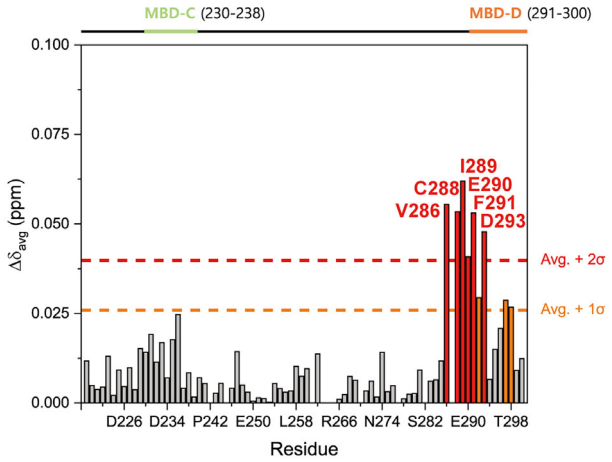

Fig. 6. Average chemical shift changes of ^{15}N labeled $BLM_{220–300}$ upon MCM6 winged-helix domain binding. Residues with $\Delta\delta_{avg}$ exceeding one standard deviation (orange bar) and two standard deviations (red bar) are highlighted. MCM6 binding domain C and D are shown at the top of the graph. NMR titration was performed once ($n = 1$) due to sample limitations. Average (Avg.) and standard deviations (σ) were calculated from the CSPs of all assigned residues.

may interact hydrophobically with the MCM6 WHD. To evaluate the interaction strength, we performed an FP assay with the $BLM_{286–300}$ peptide (Fig. S6). The results revealed a K_d value of 69.8 ± 4.5 μM, showing higher affinity compared to MBD-D ($K_d = 97.3 \pm 3.8$ μM), and highlighting the importance of the $BLM_{286–290}$ region for MCM6 WHD interaction. In contrast, the average $\Delta\delta_{avg}$ value of the MBD-C region was 0.014 ppm, and although there was a slight increase in CSP values, it did not show a significant change. Taken together, our results suggest that $BLM_{286–293}$ region is primarily involved in MCM6 WHD binding.

Discussion

In this study, we first demonstrated a correlation between MCM6 and BLM expression levels across various cancer types, including Pan-cancer data. Our findings indicate that overexpression of these proteins is associated with poorer cancer prognosis, suggesting their potential as valuable biomarkers and therapeutic targets.

FPA data revealed that MBD-C, D, and $BLM_{286–300}$ have similar K_d to MCM6 WHD, with K_ds of 83.2, 97.3, and 69.8 μM, respectively (Fig. 3A and Fig. S6). While these interactions are relatively weak, previous studies have highlighted the importance of such weak interactions in protein–protein interaction networks [64–66]. NMR spectroscopy experiments, including HSQC titration and PRE, further corroborate MCM6 WHD's preference for MBD-D over MBD-C. Although similar K_d values were obtained in the FPA experiments, we found that the presence of dimethyl sulfoxide (DMSO) likely affected the binding behavior of MBD-C observed in the NMR experiments. The FPA experiments were conducted under 10% DMSO conditions to stabilize the FITC-labeled peptide, whereas the NMR experiments were performed without DMSO. It is important to note that our study focused on specific protein domains, which may not fully capture the complexities of cellular environments, including post-translational modifications (PTM) and other protein interactions. PTMs, particularly phosphorylation of S762 and T791 in MCM6 WHD [67–71], may influence the interaction between these proteins. Although these two residues do not directly interact with MBD-D, the additional negative charges from the phosphorylation of MCM6 WHD could weaken its binding to the acidic $BLM_{220–300}$.

To better understand the evolutionary context and structural characteristics of these interactions, we conducted interspecies sequence alignments and charge distribution analyses. Interestingly, we found that MCM6 WHD is highly conserved across species, while $BLM_{220–300}$ shows greater variability (Fig. S7A,B). This conservation pattern suggests that MCM6 WHD may play a crucial role in maintaining essential functions across different organisms, while $BLM_{220–300}$ might have evolved more diverse roles or species-specific functions.

Previous interspecies sequence alignments have shown that both proteins have many negatively charged residues across species. Both proteins exhibit

low pI, with MCM6 WHD at 4.62 and $BLM_{220–300}$ at 3.97. Net charge per residue analysis revealed that MCM6 WHD possesses both negatively and positively charged surfaces, while $BLM_{220–300}$ is predominantly negatively charged (Fig. S7C,D). Notably, the helix 1 and sheet 1 regions of MCM6 WHD, which are important for BLM MBD-D interaction, are positively charged.

However, the interaction between MCM6 WHD and BLM MBD-D is not primarily charge-based. Instead, the charge distribution appears to facilitate hydrophobic interactions by preventing charge-based repulsion. This nuanced interplay between charged and hydrophobic regions highlights the complexity of protein–protein interactions. In contrast, Cdt1, another protein known to interact with MCM6 WHD [38], has a high pI value of 10.27. Our analysis confirmed that Cdt1 interacts with MCM6 WHD at a different site from BLM MBD-D (Fig. S4A,B).

This difference in binding sites can be attributed to the distinct electrostatic properties of Cdt1 compared to $BLM_{220–300}$. The positively charged Cdt1 likely interacts with the negatively charged regions of MCM6 WHD, while BLM MBD-D interacts with a different region, emphasizing the versatility of MCM6 WHD in forming protein–protein interactions. Previous studies have proposed a model in which MBD-C and D may bind to MCM6 WHD following dissociation of the MCM6 WHD-Cdt1 complex during S phase entry [56]. Our investigation suggests that BLM and Cdt1 do not share a direct binding site.

To investigate the possibility that BLM binds to other MCM WHDs, we performed structural predictions using ALPHAFOLD 3 [72]. Our results indicate that all human MCM C-terminal domains possess a WH structure (Fig. S8A). However, sequence similarity among MCM WHDs is low (Fig. S8B), and their pI values differ significantly (Fig. S8C). Although they share the same WH structure, it is unlikely that BLM will interact with all other MCMs. Cdt1 is known to interact with some WHs, but not all MCMs [35,37]. This suggests that MCM WHDs in higher organisms may have evolved diverse roles in protein–protein interactions beyond their ATPase activity, although further studies are needed to confirm this hypothesis.

Our study highlights the importance of investigating intrinsically disordered regions, despite the associated challenges. The use of NMR spectroscopy proved essential in elucidating these complex interactions. Our findings suggest that the interaction between MCM6 WHD and $BLM_{286–290}$ may be more critical than previously thought, potentially offering a new target for cancer therapeutics.

In conclusion, this study provides valuable insights into the MCM6/BLM interaction, which may guide the development of novel anticancer drugs targeting this interaction. Further research is needed to fully understand the complexities of this interaction in cellular contexts and its potential as a therapeutic target.

Materials and methods

Cohort analysis

The UCSC XENA browser (https://xena.ucsc.edu [60]) was utilized to analyze the correlation between MCM6 and BLM expression and to perform Kaplan–Meier survival analysis. Pan-cancer ($n = 11\,768$), ACC ($n = 79$), KIRC ($n = 607$), KIRP ($n = 321$), MESO ($n = 86$), LGG ($n = 529$), and GTEx database ($n = 7819$) were employed for correlation analysis. The cancer database was used to assess the survival probability of cancer patients according to MCM6 and BLM expression levels. The top 25% and bottom 25% groups of protein expression levels were used for the analysis, respectively.

Sample preparation

MCM6 WHD (residue number 708–821, C721S) was cloned into the pET His 6 GST LIC cloning vector and transformed into *Escherichia coli* BL21 (DE3) pLysS. The expression plasmid for N-His-tagged MCM6 WHD was transformed. MCM6 WHD was expressed and purified as described previously [37]. $BLM_{220–300}$ was subcloned into the pET His 6 GST LIC cloning vector and transformed into BL21 (DE3) pLysS. Site-directed mutagenesis was performed to generate $BLM_{220–300}$ C237S and C288S variants. All cells were grown at 37 °C in Lysogeny Broth (LB) medium to an optical density at 600 nm (OD_{600}) of 0.6. Protein expression was induced with 1.0 mM of isopropyl β-D-1-thiogalactopyranoside (IPTG), and cells were incubated for 20 h at 18 °C. Protein was purified with a Ni-NTA column (Cytiva, Marlborough, MA, USA) followed by gel filtration chromatography using Hi-Load 16/600 superdex 200 pg (Cytiva). The buffer composition was 20 mM 2-(N-morpholino) ethane sulfonic acid (MES), 50 mM NaCl, and 1 mM ethylenediaminetetraacetic acid (EDTA). GST-tagged protein samples were cleaved by Tobacco Etch Virus protease. ^{15}N-labeled protein samples for ^{1}H-^{15}N HSQC experiments were obtained by culturing cells in M9 minimal media containing ^{15}N-labeled NH_4Cl (Cambridge Isotope Laboratories, Tewksbury, MA, USA) as the sole nitrogen source. The overexpression and purification processes were identical to those for cells cultured in LB media. MBD-C and D peptides were commercially synthesized (BIOSTEM, Suwon, Korea).

Fluorescence polarization anisotropy assay

To determine the K_d values of MBD-C, D, and $BLM_{286–300}$ peptides with MCM6 WHD, 100 nM of BLM peptide was added with increasing concentrations of MCM6 WHD (0–2 mM) in 100 µL of buffer (20 mM MES, 50 mM NaCl, 1 mM EDTA, 10% DMSO, and pH 6.5, 1 mM dithiothreitol was included exclusively for $BLM_{286–300}$). Both peptides were FITC labeled on the N-terminal for FPA assays. FITC, a widely used fluorescence dye for FPA assays, is known to contribute partial negative charges at neutral pH. For the competitive binding assay, a mixture containing 100 nM FITC-labeled BLM MBD-C and D peptides and 200 µM MCM6 WHD was incubated with serial dilutions of unlabeled MBD-C peptide (0–4 mM) in the same buffer. The plate was mixed with a shaker for 20 min and equilibrated for 2 h at room temperature. Corning 96-well black plates were used for the FPA assay experiments. The FPA assay values were measured using Cytation 5 (BioTek, Winooski, VT, USA) and GEN5 software, with an excitation wavelength of 485 nm and an emission wavelength of 528 nm. Anisotropy values were plotted against increasing concentrations of MCM6 WHD, and the 'saturation one-site' fitting model was used to determine the K_d. Additionally, anisotropy values were plotted against increasing concentrations of BLM MBD-C peptide, and the concentration required for 50% tracer displacement was used to calculate the IC_{50}. Emission anisotropy data were analyzed using GRAPHPAD PRISM version 7.01 for Windows (GraphPad Software, San Diego, CA, USA). Experiments were performed in triplicate, and K_d and IC_{50} were calculated using the 'one-site specific' fitting model. The equation used in the fitting is as follows:

$$y = \frac{B_{max} \times x}{K_d + x}$$

$$y = -\frac{B_0 \times x}{IC_{50} + x}$$

NMR spectroscopy

NMR experiments were conducted using Bruker 900 MHz AVANCE III, 800 MHz (KBSI, Ochang, Korea), and 600 MHz (GAIA, Gwangju, Korea) NMR spectrometers equipped with cryogenic or prodigy probes. All experiments were performed in buffer containing 20 mM MES, 50 mM NaCl, and 1 mM EDTA, pH 6.5, at 298 K or 310 K. Data processing and analysis were performed using Topspin (Bruker, Billerica, MA, USA) and NMRFAM-POKY software [73]. The NMR structure and NMR chemical shift of MCM6 WHD amide nitrogen and protons were previously reported (PDB ID: 2KLQ, BMRB: 16396 [38]). Peaks that could not be matched to published values were assigned by performing NNH-NOESY experiments. We performed the backbone assignment of BLM (220–300; BMRB: 52084 [59]). ^{1}H-^{15}N HSQC titration experiments were performed by adding 0, 300, 600, and 1200 µM unlabeled MBD-D or 600 µM unlabeled MBD-C to 300 µM ^{15}N-labeled MCM6 WHD, and by adding 0, 125, 250, and 500 µM unlabeled MCM6 WHD to 250 µM ^{15}N-labeled $BLM_{220–300}$. $\Delta\delta_{avg}$ were calculated using the following equation:

$$\Delta\delta_{avg} = \sqrt{(\Delta\delta_H)^2 + \left(\frac{\Delta\delta_N}{5.88}\right)^2}$$

$\Delta\delta_H$ and $\Delta\delta_N$ are the chemical shift changes of the amide proton and nitrogen, respectively.

For PRE experiments, $BLM_{220–300}$ C238S and $BLM_{220–300}$ C288S were labeled MTSL [74]. Experiments were conducted with 100 µM of ^{15}N-labeled MCM6 WHD and 100 µM of MTSL-labeled $BLM_{220–300}$ C238S or $BLM_{220–300}$ C288S. To obtain the diamagnetic state spectrum, 0.5 mM of ascorbic acid (from a 250 mM stock) was added to the sample and incubated for 3 h at room temperature before NMR measurements. PRE measurements were performed by acquiring two sets of ^{1}H-^{15}N HSQC spectra from the identical sample, before and after reducing the spin-label. Peak intensities were quantified and represented as the ratio of intensities between the oxidized state (I_{ox}) and the reduced state (I_{red}).

Acknowledgements

We thank the high-field NMR facility at the Korean Basic Science Institute (KBSI, Ochang) and the GIST Advanced Institute of Instrumental Analysis (GAIA, Gwangju) for their assistance with NMR experiments; Prof Min-Gon Kim for providing access to the Cytation 5 instrument for the FPA experiments; Mr Seho Park for his help with the UCSC XENA cohort analysis. The authors used Claude (Anthropic, San Francisco, CA, USA) and ChatGPT (OpenAI, San Francisco, CA, USA) to refine the language and improve the clarity of this article. The authors reviewed and edited the AI-generated output and take full responsibility for the content of the publication. This work was supported by the National Research Foundation (NRF) of Korea grant number (2021R1A2C1004669 and RS-2024-00411137 to C-JP), which is funded by the Korean government (MSIT); and by the Korea Basic Science Institute under the R&D program (Project No. A412550) supervised by the Ministry of Science and ICT, Korea.

Conflict of interest

The authors declare no conflict of interest.

Author contributions

MJY: Conceptualization, formal analysis, investigation, validation, writing–original draft, writing–review

and editing. HL: Formal analysis, investigation, validation, writing–original draft. DK: Investigation, validation. C-JP: Conceptualization, funding acquisition, supervision, writing–review and editing.

Peer review

The peer review history for this article is available at https://www.webofscience.com/api/gateway/wos/peer-review/10.1111/febs.70047.

Data availability statement

The data that support the findings of the present study are available from the corresponding author (cjpark@gist.ac.kr) upon reasonable request.

References

1 Helleday T, Lo J, van Gent DC & Engelward BP (2007) DNA double-strand break repair: from mechanistic understanding to cancer treatment. *DNA Repair* **6**, 923–935.
2 Aguilera A & Gómez-González B (2008) Genome instability: a mechanistic view of its causes and consequences. *Nat Rev Genet* **9**, 204–217.
3 Daley JM, Chiba T, Xue X, Niu H & Sung P (2014) Multifaceted role of the topo IIIα–RMI1-RMI2 complex and DNA2 in the BLM-dependent pathway of DNA break end resection. *Nucleic Acids Res* **42**, 11083–11091.
4 Mao Z, Bozzella M, Seluanov A & Gorbunova V (2008) Comparison of nonhomologous end joining and homologous recombination in human cells. *DNA Repair* **7**, 1765–1771.
5 Karow JK, Constantinou A, Li J-L, West SC & Hickson ID (2000) The Bloom's syndrome gene product promotes branch migration of Holliday junctions. *Proc Natl Acad Sci U S A* **97**, 6504–6508.
6 Roy R, Chun J & Powell SN (2011) BRCA1 and BRCA2: different roles in a common pathway of genome protection. *Nat Rev Cancer* **12**, 68–78.
7 Prakash R, Zhang Y, Feng W & Jasin M (2015) Homologous recombination and human health: the roles of BRCA1, BRCA2, and associated proteins. *Cold Spring Harb Perspect Biol* **7**, a016600.
8 Lombard DB, Chua KF, Mostoslavsky R, Franco S, Gostissa M & Alt FW (2005) DNA repair, genome stability, and aging. *Cell* **120**, 497–512.
9 Drissi R, Chauvin A, McKenna A, Lévesque D, Blais-Brochu S, Jean D & Boisvert FM (2018) Destabilization of the MiniChromosome maintenance (MCM) complex modulates the cellular response to DNA double strand breaks. *Cell Cycle* **17**, 2593–2609.
10 Evrin C, Clarke P, Zech J, Lurz R, Sun J, Uhle S, Li H, Stillman B & Speck C (2009) A double-hexameric MCM2-7 complex is loaded onto origin DNA during licensing of eukaryotic DNA replication. *Proc Natl Acad Sci U S A* **106**, 20240–20245.
11 Schwacha A & Bell SP (2001) Interactions between two catalytically distinct MCM subgroups are essential for coordinated ATP hydrolysis and DNA replication. *Mol Cell* **8**, 1093–1104.
12 Xu X, Rochette PJ, Feyissa EA, Su TV & Liu Y (2009) MCM10 mediates RECQ4 association with MCM2-7 helicase complex during DNA replication. *EMBO J* **28**, 3005–3014.
13 Li N, Zhai Y, Zhang Y, Li W, Yang M, Lei J, Tye B-K & Gao N (2015) Structure of the eukaryotic MCM complex at 3.8 Å. *Nature* **524**, 186–191.
14 Yu S, Wang G, Shi Y, Xu H, Zheng Y & Chen Y (2020) MCMs in cancer: prognostic potential and mechanisms. *Anal Cell Pathol (Amst)* **2020**, 3750294.
15 Masai H, Matsumoto S, You Z, Yoshizawa-Sugata N & Oda M (2010) Eukaryotic chromosome DNA replication: where, when, and how? *Annu Rev Biochem* **79**, 89–130.
16 He DM, Ren BG, Liu S, Tan LZ, Cieply K, Tseng G, Yu YP & Luo JH (2017) Oncogenic activity of amplified miniature chromosome maintenance 8 in human malignancies. *Oncogene* **36**, 3629–3639.
17 Chuang CH, Wallace MD, Abratte C, Southard T & Schimenti JC (2010) Incremental genetic perturbations to MCM2-7 expression and subcellular distribution reveal exquisite sensitivity of mice to DNA replication stress. *PLoS Genet* **6**, e1001110.
18 Fu Y, Zhou QZ, Zhang XL, Wang ZZ & Wang P (2019) Identification of hub genes using Co-expression network analysis in breast cancer as a tool to predict different stages. *Med Sci Monit* **25**, 8873–8890.
19 Cheng L, Tan Z, Huang Z, Pan Y, Zhang W & Wang J (2020) Expression profile and prognostic values of mini-chromosome maintenance families (MCMs) in breast cancer. *Med Sci Monit* **26**, e923673.
20 Sadeghian D, Saffar H, Mahdavi Sharif P, Soleimani V & Jahanbin B (2022) MCM6 versus Ki-67 in diagnosis of luminal molecular subtypes of breast cancers. *Diagn Pathol* **17**, 24.
21 Chen QY, Liu LC, Wang JB, Xie JW, Lin JX, Lu J, Cao LL, Lin M, Tu RH, Huang CM *et al.* (2019) CDK5RAP3 inhibits the translocation of MCM6 to influence the prognosis in gastric cancer. *J Cancer* **10**, 4488–4498.
22 Wang Y, Chen H, Liu W, Yan H, Zhang Y, Cheung AHK, Zhang J, Chen B, Liang L, Zhou Z *et al.* (2022) MCM6 is a critical transcriptional target of YAP to promote gastric tumorigenesis and serves as a therapeutic target. *Theranostics* **12**, 6509–6526.

23 Jang NR, Baek J, Ko Y, Song PH & Gu MJ (2021) High MCM6 expression as a potential prognostic marker in clear-cell renal cell carcinoma. *In Vivo* **35**, 299–306.
24 Zhang J, Zhang H, Wang Y & Wang Q (2021) MCM2-7 in clear cell renal cell carcinoma: MCM7 promotes tumor cell proliferation. *Front Oncol* **11**, 782755.
25 Zhong H, Chen B, Neves H, Xing J, Ye Y, Lin Y, Zhuang G, Zhang SD, Huang J & Kwok HF (2017) Expression of minichromosome maintenance genes in renal cell carcinoma. *Cancer Manag Res* **9**, 637–647.
26 Hou L, Zeng X, Li X, Zhao C, Zou J, Li Y & Liu G (2022) MCM6 promotes hepatocellular carcinoma progression via the notch pathway: clinical, functional, and genomic insights. *Comput Math Methods Med* **2022**, 3116303.
27 Zeng T, Guan Y, Li YK, Wu Q, Tang XJ, Zeng X, Ling H & Zou J (2021) The DNA replication regulator MCM6: an emerging cancer biomarker and target. *Clin Chim Acta* **517**, 92–98.
28 Zheng T, Chen M, Han S, Zhang L, Bai Y, Fang X, Ding SZ & Yang Y (2014) Plasma minichromosome maintenance complex component 6 is a novel biomarker for hepatocellular carcinoma patients. *Hepatol Res* **44**, 1347–1356.
29 Liao X, Liu X, Yang C, Wang X, Yu T, Han C, Huang K, Zhu G, Su H, Qin W *et al.* (2018) Distinct diagnostic and prognostic values of Minichromosome maintenance gene expression in patients with hepatocellular carcinoma. *J Cancer* **9**, 2357–2373.
30 Liu YZ, Wang BS, Jiang YY, Cao J, Hao JJ, Zhang Y, Xu X, Cai Y & Wang MR (2017) MCMs expression in lung cancer: implication of prognostic significance. *J Cancer* **8**, 3641–3647.
31 Kadara H, Lacroix L, Behrens C, Solis L, Gu X, Lee JJ, Tahara E, Lotan D, Hong WK, Wistuba II *et al.* (2009) Identification of gene signatures and molecular markers for human lung cancer prognosis using an in vitro lung carcinogenesis system. *Cancer Prev Res* **2**, 702–711.
32 Vigouroux C, Casse J-M, Battaglia-Hsu S-F, Brochin L, Luc A, Paris C, Lacomme S, Gueant J-L, Vignaud J-M & Gauchotte G (2015) Methyl(R217)HuR and MCM6 are inversely correlated and are prognostic markers in non small cell lung carcinoma. *Lung Cancer* **89**, 189–196.
33 Song HY, Shen R, Mahasin H, Guo YN & Wang DG (2023) DNA replication: mechanisms and therapeutic interventions for diseases. *MedComm* **4**, e210.
34 Hotton J, Agopiantz M, Leroux A, Charra-Brunaud C, Marie B, Busby-Venner H, Morel O, Guéant JL, Vignaud JM, Battaglia-Hsu SF *et al.* (2018) Minichromosome maintenance complex component 6 (MCM6) expression correlates with histological grade and survival in endometrioid endometrial adenocarcinoma. *Virchows Arch* **472**, 623–633.
35 Guerrero-Puigdevall M, Fernandez-Fuentes N & Frigola J (2021) Stabilisation of half MCM ring by Cdt1 during DNA insertion. *Nat Commun* **12**, 1746.
36 Zeng H, Li J, Xu H, Li H & Liu Y (2020) Crystal structure of the winged-helix domain of MCM8. *Biochem Biophys Res Commun* **526**, 993–998.
37 Liu C, Wu R, Zhou B, Wang J, Wei Z, Tye BK, Liang C & Zhu G (2012) Structural insights into the Cdt1-mediated MCM2–7 chromatin loading. *Nucleic Acids Res* **40**, 3208–3217.
38 Wei Z, Liu C, Wu X, Xu N, Zhou B, Liang C & Zhu G (2010) Characterization and structure determination of the Cdt1 binding domain of human minichromosome maintenance (mcm) 6. *J Biol Chem* **285**, 12469–12473.
39 Karow JK, Chakraverty RK & Hickson ID (1997) The Bloom's syndrome gene product is a 3′–5′ DNA helicase. *J Biol Chem* **272**, 30611–30614.
40 German J, Roe AM, Leppert MF & Ellis NA (1994) Bloom syndrome: an analysis of consanguineous families assigns the locus mutated to chromosome band 15q26. 1. *Proc Natl Acad Sci U S A* **91**, 6669–6673.
41 Machwe A, Xiao L, Groden J & Orren DK (2006) The Werner and Bloom syndrome proteins catalyze regression of a model replication fork. *Biochemistry* **45**, 13939–13946.
42 Heyer WD, Ehmsen KT & Liu J (2010) Regulation of homologous recombination in eukaryotes. *Annu Rev Biochem* **44**, 113–139.
43 Cortez D (2019) Replication-coupled DNA repair. *Mol Cell* **74**, 866–876.
44 Friedberg EC (2003) DNA damage and repair. *Nature* **421**, 436–440.
45 Jackson SP & Bartek J (2009) The DNA-damage response in human biology and disease. *Nature* **461**, 1071–1078.
46 Davies SL, North PS & Hickson ID (2007) Role for BLM in replication-fork restart and suppression of origin firing after replicative stress. *Nat Struct Mol Biol* **14**, 677–679.
47 Newman JA, Savitsky P, Allerston CK, Bizard AH, Özer Ö, Sarlós K, Liu Y, Pardon E, Steyaert J, Hickson ID *et al.* (2015) Crystal structure of the Bloom's syndrome helicase indicates a role for the HRDC domain in conformational changes. *Nucleic Acids Res* **43**, 5221–5235.
48 Neuwald AF, Aravind L, Spouge JL & Koonin EV (1999) AAA+: a class of chaperone-like ATPases associated with the assembly, operation, and disassembly of protein complexes. *Genome Res* **9**, 27–43.
49 Kedzierska S (2006) Structure, function and mechanisms of action of ATPases from the AAA superfamily of proteins. *Postepy Biochem* **52**, 330–338.

50 Spiegel J, Adhikari S & Balasubramanian S (2020) The structure and function of DNA G-Quadruplexes. *Trends Chem* **2**, 123–136.
51 Wu WQ, Hou XM, Li M, Dou SX & Xi XG (2015) BLM unfolds G-quadruplexes in different structural environments through different mechanisms. *Nucleic Acids Res* **43**, 4614–4626.
52 Thakkar MK, Lee J, Meyer S & Chang VY (2022) RecQ helicase somatic alterations in cancer. *Front Mol Biosci* **9**, 887758.
53 Guo Y, Xu H, Huang M & Ruan Y (2023) BLM promotes malignancy in PCa by inducing KRAS expression and RhoA suppression via its interaction with HDGF and activation of MAPK/ERK pathway. *J Cell Commun Signal* **17**, 757–772.
54 Votino C, Laudanna C, Parcesepe P, Giordano G, Remo A, Manfrin E & Pancione M (2017) Aberrant BLM cytoplasmic expression associates with DNA damage stress and hypersensitivity to DNA-damaging agents in colorectal cancer. *J Gastroenterol* **52**, 327–340.
55 Zhou B-BS & Elledge SJ (2000) The DNA damage response: putting checkpoints in perspective. *Nature* **408**, 433–439.
56 Shastri VM, Subramanian V & Schmidt KH (2021) A novel cell-cycle-regulated interaction of the bloom syndrome helicase BLM with Mcm6 controls replication-linked processes. *Nucleic Acids Res* **49**, 8699–8713.
57 Mao Z, Bozzella M, Seluanov A & Gorbunova V (2008) DNA repair by nonhomologous end joining and homologous recombination during cell cycle in human cells. *Cell Cycle* **7**, 2902–2906.
58 Kim YM & Choi BS (2010) Structure and function of the regulatory HRDC domain from human bloom syndrome protein. *Nucleic Acids Res* **38**, 7764–7777.
59 Yang MJ & Park CJ (2023) Backbone assignment of the intrinsically disordered N-terminal region of bloom syndrome protein. *J Korean Magn Reson Soc* **27**, 17–22.
60 Goldman MJ, Craft B, Hastie M, Repečka K, McDade F, Kamath A, Banerjee A, Luo Y, Rogers D, Brooks AN *et al.* (2020) Visualizing and interpreting cancer genomics data via the Xena platform. *Nat Biotechnol* **38**, 675–678.
61 Hanahan D & Weinberg RA (2011) Hallmarks of cancer: the next generation. *Cell* **144**, 646–674.
62 Yao B, Hu W, Chen Y, Li J, Jiang K & Dou J (2024) Pan-cancer analysis of the TRAF family genes and their correlation with prognosis, TME, immune and drug sensitivity. *Eur J Med Res* **29**, 307.
63 Clore GM & Iwahara J (2009) Theory, practice, and applications of paramagnetic relaxation enhancement for the characterization of transient Low-population states of biological macromolecules and their complexes. *Chem Rev* **109**, 4108–4139.
64 Pawson T & Scott JD (2005) Protein phosphorylation in signaling--50 years and counting. *Trends Biochem Sci* **30**, 286–290.
65 Ellis RJ (2001) Macromolecular crowding: obvious but underappreciated. *Trends Biochem Sci* **26**, 597–604.
66 De Las Rivas J & Fontanillo C (2010) Protein–protein interactions essentials: key concepts to building and analyzing Interactome networks. *PLoS Comput Biol* **6**, e1000807.
67 Beausoleil SA, Villén J, Gerber SA, Rush J & Gygi SP (2006) A probability-based approach for high-throughput protein phosphorylation analysis and site localization. *Nat Biotechnol* **24**, 1285–1292.
68 Dephoure N, Zhou C, Villén J, Beausoleil SA, Bakalarski CE, Elledge SJ & Gygi SP (2008) A quantitative atlas of mitotic phosphorylation. *Proc Natl Acad Sci U S A* **105**, 10762–10767.
69 Mayya V, Lundgren DH, Hwang SI, Rezaul K, Wu L, Eng JK, Rodionov V & Han DK (2009) Quantitative phosphoproteomic analysis of T cell receptor signaling reveals system-wide modulation of protein-protein interactions. *Sci Signal* **2**, ra46.
70 Olsen JV, Vermeulen M, Santamaria A, Kumar C, Miller ML, Jensen LJ, Gnad F, Cox J, Jensen TS, Nigg EA *et al.* (2010) Quantitative phosphoproteomics reveals widespread full phosphorylation site occupancy during mitosis. *Sci Signal* **3**, ra3.
71 Zhou H, Di Palma S, Preisinger C, Peng M, Polat AN, Heck AJ & Mohammed S (2013) Toward a comprehensive characterization of a human cancer cell phosphoproteome. *J Proteome Res* **12**, 260–271.
72 Abramson J, Adler J, Dunger J, Evans R, Green T, Pritzel A, Ronneberger O, Willmore L, Ballard AJ, Bambrick J *et al.* (2024) Accurate structure prediction of biomolecular interactions with AlphaFold 3. *Nature* **630**, 493–500.
73 Lee W, Rahimi M, Lee Y & Chiu A (2021) POKY: a software suite for multidimensional NMR and 3D structure calculation of biomolecules. *Bioinformatics* **37**, 3041–3042.
74 Sjodt M & Clubb RT (2017) Nitroxide labeling of proteins and the determination of paramagnetic relaxation derived distance restraints for NMR studies. *Bio Protoc* **7**, e2207.
75 Schrödinger, LLC (2015) The PyMOL Molecular Graphics System, Version 3.1.3.

Supporting information

Additional supporting information may be found online in the Supporting Information section at the end of the article.

Fig. S1. Correlation between MCM6 and BLM expression levels in various cancer cell types.

Fig. S2. Overlaid ^{1}H-^{15}N HSQC spectra of ^{15}N-labeled MCM6 WHD titrated with a twofold molar excess of BLM MBD-C peptide.

Fig. S3. Overlaid ^{1}H-^{15}N HSQC spectra of ^{15}N-labeled MCM6 WHD titrated with increasing concentrations of BLM MBD-D peptide.
Fig. S4. Structural analysis of MCM6 WHD, including interactions, electrostatics, and hydrophobicity.
Fig. S5. Overlaid ^{1}H-^{15}N HSQC spectra of ^{15}N-labeled $BLM_{220–300}$ titrated with increasing concentrations of MCM6 WHD.
Fig. S6. Fluorescence polarization anisotropy of FITC-labeled $BLM_{286–300}$ titrated by MCM6 WHD.
Fig. S7. Evolutionary conservation and charge distribution of MCM6 WHD and $BLM_{220–300}$.
Fig. S8. Prediction structures, sequence alignments, and charge properties of MCM2-7 WHDs.